Activation of Tri(2-furyl)phosphine by $[Ru_4(\mu\text{-}H)_4(CO)_{12}]$: The First Example of Coordinated Furyl and Furyne Ligands at Tetraruthenium Phosphide and Phosphinidene Clusters

Wai-Yeung Wong* and Fai-Lung Ting

Department of Chemistry, Hong Kong Baptist University, Waterloo Road, Kowloon Tong, Hong Kong, People's Republic of China

Zhenyang Lin

Department of Chemistry, The Hong Kong University of Science and Technology, Clearwater Bay, Hong Kong, People's Republic of China

Received August 21, 2003

Tri(2-furyl)phosphine (PFu_3) reacts with $[Ru_4(\mu\text{-}H)_4(CO)_{12}]$ (**1**) in refluxing THF to give, apart from an isomeric pair of the substituton products $[Ru_4(\mu\text{-}H)_4(CO)_{10}(PFu_3)_2]$ (**2a** and **2b**), the μ-phosphido cluster $[Ru_4(\mu\text{-}H)_2(CO)_8(PFu_3)_2(\mu\text{-}PFu_2)(\mu\text{-}\eta^1,\eta^2\text{-}C_4H_3O)]$ (**3**) and a series of μ_3- and μ_4-phosphinidene clusters $[Ru_4(\mu\text{-}H)_2(CO)_{12-x}(PFu_3)_x(\mu_3\text{-}PFu)]$ ($x = 0$ (**4**), 2 (**5**), 3 (**6**)) and $[Ru_4(\mu\text{-}H)_2(CO)_9(PFu_3)_2(\mu_4\text{-}PFu)(\mu_3\text{-}\eta^1,\eta^1,\eta^2\text{-}C_4H_2O)]$ (**7**). In this one-pot reaction, the excellent facility for PFu_3 to act as rich sources of furyl, furyne, phosphide (μ-PR_2), and phosphinidene (μ_3-PR and μ_4-PR) fragments on tetrametallic frameworks has been demonstrated. The single-crystal X-ray structures of all new molecules have been determined. The structure of **7** represents the first structurally characterized example of stable furyne-containing cluster complexes of ruthenium. The electrochemical behavior and molecular orbital calculations of these metallophosphorus clusters have been examined as a function of the coordination modes of the phosphorus-containing moieties.

Introduction

In recent years, work has proliferated in the area of transition metal carbonyl clusters containing main group ligands.[1,2] A wide range of such clusters of the iron triad that possess terminal, edge-bridged, and capped phosphine ligands have been prepared from the reactions of alkyl or aryl tertiary phosphines with appropriate metal carbonyl clusters,[1,2] and examples of facile P−C bond formation and cleavage,[3] alkyne oligomerization,[4] and skeletal transformations[5] are well known. Specifically, considerable recent effort has been devoted to the reactivity studies of phosphine ligands with additional donor sites toward multinuclear metal carbonyls.[3a,6] In this connection, the chemistry of phosphine ligands bearing thienyl and pyrrolyl substituents has come under intense scrutiny on account of their respective importance in the hydrodesulfurization[7] and hydrodenitrogenation[8] processes in industry, and sev-

* To whom correspondence should be addressed. E-mail: rwywong@hkbu.edu.hk.

(1) See for example: (a) Huttner, G.; Knoll, K. *Angew. Chem., Int. Ed. Engl.* **1987**, *26*, 743. (b) O'Neill, M. E.; Wade, K. *Metal Interactions with Boron Clusters*; Grimes, R. N., Ed.; Plenum Press: New York, 1982. (c) *Transition Metal Clusters*; Johnson, B. F. G., Ed.; Wiley: New York, 1980. (d) Vahrenkamp, H. *Adv. Organomet. Chem.* **1983**, *22*, 169. (e) Adams, R. D.; Horvath, I. T. *Prog. Inorg. Chem.* **1985**, *33*, 127. (f) *Metal Clusters in Chemistry*; Braunstein, P., Oro, L. A., Raithby, P. R., Ed.; Wiley-VCH: New York, 1999; Vols. 1−3. (g) Whitmire, K. H. *Adv. Organomet. Chem.* **1997**, *42*, 1.

(2) See for example: (a) Ang, H. G.; Ang, S. G.; Du, S.; Sow, B. H.; Wu, X. *J. Chem. Soc., Dalton Trans.* **1999**, 2799. (b) Süss-Fink, G.; Godefroy, I.; Béguin, A.; Rheinwald, G.; Neels, A.; Stoeckli-Evans, H. *J. Chem. Soc., Dalton Trans.* **1998**, 2211. (c) Wang, W.; Enright, G. D.; Carty, A. J. *J. Am. Chem. Soc.* **1997**, *119*, 12370. (d) Wang, W.; Corrigan, J. F.; Enright, G. D.; Taylor, N. J.; Carty, A. J. *Organometallics* **1998**, *17*, 427. (e) Zheng, T. C.; Cullen, W. R.; Rettig, S. J. *Organometallics* **1994**, *13*, 3594. (f) Cherkas, A. A.; Corrigan, J. F.; Doherty, S.; MacLaughlin, S. A.; van Gastel, F.; Taylor, N. J.; Carty, A. J. *Inorg. Chem.* **1993**, *32*, 1662. (g) Knox, S. A. R.; Lloyd, B. R.; Morton, D. A. V.; Nicholls, S. M.; Orpen, A. J.; Viñas, J. M.; Weber, M.; Williams, G. K. *J. Organomet. Chem.* **1990**, *394*, 385. (h) Bruce, M. I.; Liddell, M. J.; Tiekink, E. R. T. *J. Organomet. Chem.* **1990**, *391*, 81.

(3) (a) Lugan, N.; Lavigne, G.; Bonnet, J.-J. *Inorg. Chem.* **1987**, *26*, 585. (b) Bergounhou, C.; Bonnet, J.-J.; Fompeyrine, P.; Lavigne, G.; Lugan, N.; Mansilla, F. *Organometallics* **1986**, *5*, 60.

(4) (a) Ang, H. G.; Ang, S. G.; Du, S. *J. Chem. Soc., Dalton Trans.* **1999**, 2963. (b) Chi, Y.; Carty, A. J.; Blenkiron, P.; Delgado, E.; Enright, G. D.; Wang, W.; Peng, S.-M.; Lee, G.-H. *Organometallics* **1996**, *15*, 5269. (c) Clarke, L. P.; Davies, J. E.; Raithby, P. R.; Shields, G. P. *J. Chem. Soc., Dalton Trans.* **2000**, 4527. (d) Corrigan, J. F.; Taylor, N. J.; Carty, A. J. *Organometallics* **1994**, *13*, 376. (e) Corrigan, J. F.; Doherty, S.; Taylor, N. J.; Carty, A. J. *Organometallics* **1993**, *12*, 1365.

(5) Tseng, W.-C.; Chi, Y.; Su, C.-J.; Carty, A. J.; Peng, S.-M.; Lee, G.-H. *J. Chem. Soc., Dalton Trans.* **1998**, 1053.

(6) (a) Deeming, A. J.; Jayasuriya, S. N.; Arce, A. J.; Sanctis, Y. D. *Organometallics* **1996**, *15*, 786. (b) Bodensieck, U.; Vahrenkamp, H.; Rheinwald, G.; Stoeckli-Evans, H. *J. Organomet. Chem.* **1995**, *488*, 85. (c) Arce, A. J.; Deeming, A. J.; Sanctis, Y. D.; Johal, S. K.; Martin, C. M.; Shinhmar, M.; Speel, D. M.; Vassos, A. *Chem. Commun.* **1998**, 233. (d) Braunstein, P.; Coco Cea, S.; Bruce, M. I.; Skelton, B. W.; White, A. H. *J. Organomet. Chem.* **1992**, *423*, C38. (e) Adams, C. J.; Bruce, M. I.; Duckworth, P. A.; Humphrey, P. A.; Kuhl, O.; Tiekink, E. R. T.; Cullen, W. R.; Braunstein, P.; Coco Cea, S.; Skelton, B. W.; White, A. H. *J. Organomet. Chem.* **1994**, *467*, 251.

(7) Angelici, R. J. In *Encyclopedia of Inorganic Chemistry*; King, R. B., Ed.; Wiley: New York, 1994; Vol. 3, pp 1433−1443.

(8) (a) Laine, R. M. *Ann. N. Y. Acad. Sci.* **1983**, *415*, 271. (b) Fish, R. H. *Ann. N. Y. Acad. Sci.* **1983**, *415*, 292. (c) Eisenstadt, A.; Giandomenico, C. M.; Frederick, M. F.; Laine, R. M. *Organometallics* **1985**, *4*, 2033. (d) Chisholm, M. H. *Polyhedron* **1997**, *16*, 3071, and various articles cited in this Symposium-in-Print.

10.1021/om0341193 CCC: $25.00
Publication on Web 10/25/2003

eral recent developments provide a wealth of intriguing reactivity of these phosphines toward metal carbonyl clusters.[6a−c] Deeming and co-workers have shown that thermal reaction of the cyclometalated compound $[Ru_3(\mu\text{-H})(CO)_9(\mu_3\text{-}Ph_2PC_4H_2S)]$ with $[Ru_3(CO)_{12}]$ produced the μ_4-thiophyne complex $[Ru_4(CO)_{11}(\mu_4\text{-PPh})(\mu_4\text{-}C_4H_2S)]$ and the μ_4-benzyne complex $[Ru_4(CO)_{11}(\mu_4\text{-PPh})(\mu_4\text{-}C_6H_4)]$ by elimination of benzene and thiophene, respectively.[6a] Moreover, a donor-induced cluster degradation product, $[Ru(CO)_3\{P(C_4H_3S)_3\}_2]$, was formed from the reaction between $[Ru_3(CO)_{12}]$ and tri(2-thienyl)phosphine.[6b] Likewise, two isomeric clusters $[Ru_4(CO)_{11}(\mu_4\text{-PPh})(\mu_4\text{-}C_4H_3N)]$, which contain the pyrrolyne ligands, were isolated upon treatment of $[Ru_3(CO)_{12}]$ with pyrrolyl phosphines.[6c] Although the use of tri(2-furyl)phosphine (PFu_3) as a reagent for transition metal-mediated synthesis has been documented,[9] relatively little attention has been paid to the reactivity studies between polynuclear metal clusters and phosphines involving a furan group, an oxygen analogue of thiophene and pyrrole. Our recent interest in the employment of PFu_3 as a ligand in organometallic syntheses[10] prompted us to explore whether this phosphine can be a versatile polyfunctional ligand to afford phosphorus-rich metal cluster complexes with novel coordination modes. We now report a detailed account of the reaction of $[Ru_4(\mu\text{-H})_4(CO)_{12}]$ with PFu_3, whereupon a facile and convenient synthetic route to a series of μ-phosphide and μ_n-phosphinidene ($n = 3, 4$) tetraruthenium hydrido clusters has been developed. The electrochemistry of these complexes was studied using cyclic voltammetry as well as controlled-potential coulometry, and the results were correlated to theoretical calculations by the method of density functional theory.

Results and Discussion

Reaction of $[Ru_4(\mu\text{-H})_4(CO)_{12}]$ with Tri(2-furyl)phosphine. The reaction of $[Ru_4(\mu\text{-H})_4(CO)_{12}]$ with tri(2-furyl)phosphine (PFu_3) in THF at reflux temperature for 3 h generated seven new products in low to moderate yields (Scheme 1). The products were separated by preparative thin-layer chromatography (TLC) followed by recrystallization, and they are stable as solids in the air and soluble in common organic solvents. They were fully characterized using FAB mass spectrometry, IR and NMR spectroscopies, and single-crystal X-ray diffraction. In this single reaction, seven tetraruthenium hydrido clusters were isolated and identified as the two isomeric clusters $[Ru_4(\mu\text{-H})_4(CO)_{10}(PFu_3)_2]$ (**2a** and **2b**), the μ-phosphido-stabilized cluster $[Ru_4(\mu\text{-H})_2(CO)_8(PFu_3)_2(\mu\text{-}PFu_2)(\mu\text{-}\eta^1,\eta^2\text{-}C_4H_3O)]$ (**3**), and a series of μ_3- and μ_4-phosphinidene clusters $[Ru_4(\mu\text{-H})_2(CO)_{12-x}(PFu_3)_x(\mu_3\text{-PFu})]$ ($x = 0$ (**4**), 2 (**5**), 3 (**6**)) and $[Ru_4(\mu\text{-H})_2(CO)_9(PFu_3)_2(\mu_4\text{-PFu})(\mu_3\text{-}\eta^1,\eta^1,\eta^2\text{-}C_4H_2O)]$ (**7**). A few minor products remain unidentified in this reaction. The overall product yields of **3**−**7** amount to ca. 51%, which do not seem to vary much with the reaction stoichiometry. Their respective yields depend, to a certain extent, on the reaction conditions and the time of reflux. Increased reaction time or temperature provided a higher proportion of **5** and **6** at the expense of **4**. The generation of **5** and **6** can also be effected by the reaction of **4** with excess PFu_3. However, the mechanism for this reaction is not clear at present, and there is no direct evidence for the interconversion among **3**, **5**, and **7**. We also did not observe the formation of **3** directly from the reaction of **2a** or **2b** with PFu_3.

Scheme 1

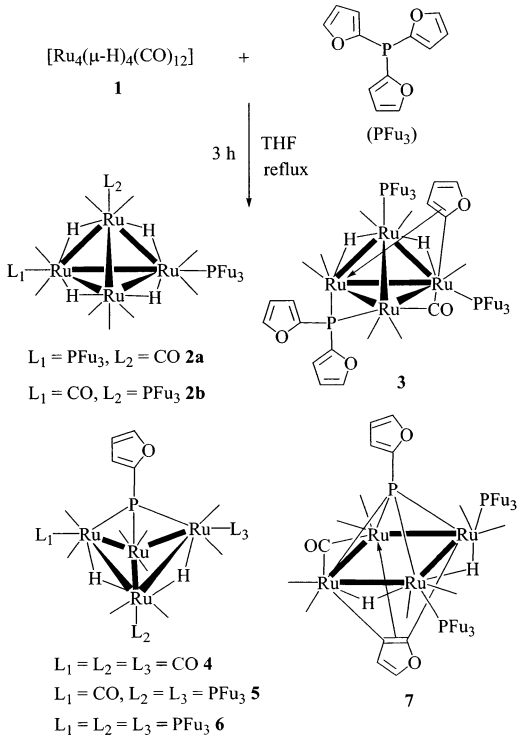

Spectroscopic and Structural Characterization of 2a and 2b. Both **2a** and **2b** possess slightly different NMR spectra, yet identical molecular ion peaks at m/z 1152 are observed in their mass spectra. Proton resonances arising from the furyl groups are observed in the ^1H NMR spectra, and each of their $^{31}P\{^1H\}$ NMR spectra shows a singlet peak that is shifted downfield relative to the value of δ −75.8 ppm for the free phosphine ligand. Both compounds show only terminal carbonyl absorptions, reminiscent of other $[Ru_4(\mu\text{-H})_4(CO)_{10}(PR_3)_2]$ (R = alkyl, aryl) complexes known in the literature.[11a−d]

Crystal structure analyses of **2a** and **2b** were carried out, and their molecular structures are shown in Figures 1 and 2, respectively. Selected bond lengths and angles are collected in Table 1. The metal skeleton of both complexes is based on a Ru_4 tetrahedron with 10 terminal carbonyl ligands, four bridging hydrides, and two substituted phosphines, but the spatial positions of the phosphines are different. A formal electron count indicates that **2a** and **2b** are both 60-electron species, in agreement with the EAN rule for a tetrahedral core. Both molecules exhibit the characteristic four-long/two-short pattern of Ru−Ru distances.[11] The long distances Ru(1)−Ru(2) 2.9492(3) (2.9707(3)), Ru(2)−Ru(3) 2.9616(3) (2.9556(3)), Ru(3)−Ru(4) 2.9671(3) (2.9539(3)), and Ru(1)−Ru(4) 2.9785(3) (2.9806(3)) Å for **2a** (**2b**) correspond to the Ru−H−Ru bonds, while the short distances for Ru(1)−Ru(3) (2.7875(3) **2a**; 2.7913(3) Å **2b**) and Ru(2)−Ru(4) (2.7775(3) **2a**; 2.7768(3) Å **2b**) are due

(9) Andersen, N. G.; Keay, B. A. *Chem. Rev.* **2001**, *101*, 997.
(10) (a) Wong, W.-Y.; Ting, F.-L.; Lam, W.-L. *J. Chem. Soc., Dalton Trans.* **2001**, 2981. (b) Wong, W.-Y.; Ting, F.-L.; Lam, W.-L. *Eur. J. Inorg. Chem.* **2002**, 2103.

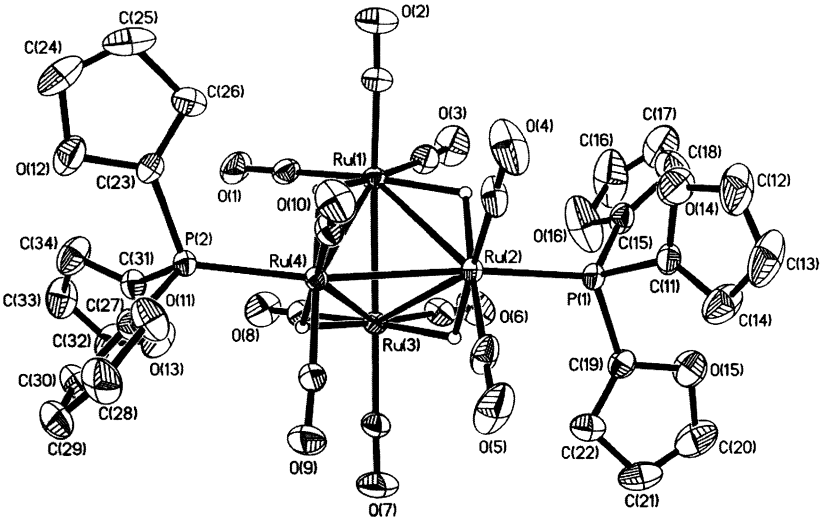

Figure 1. Molecular structure of **2a** with 25% probability ellipsoids. For clarity, all H atoms on the furyl rings are omitted and the labels on the carbonyl C atoms have the same labels as the O atoms.

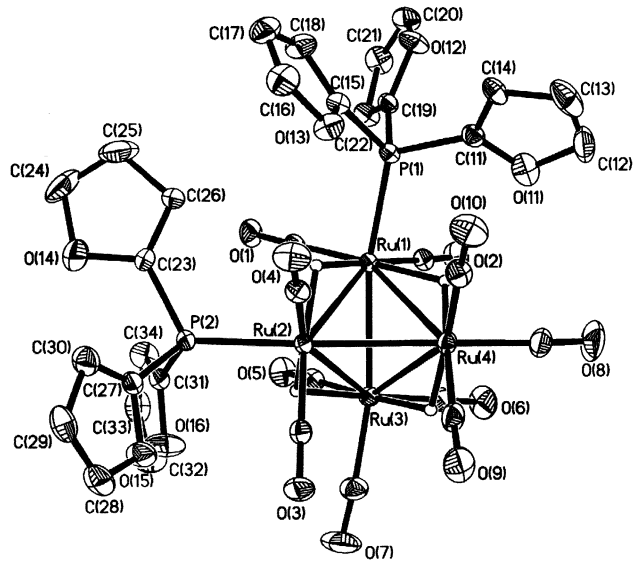

Figure 2. Molecular structure of **2b** with 25% probability ellipsoids. For clarity, all H atoms on the furyl rings are omitted and the labels on the carbonyl C atoms have the same labels as the O atoms.

Table 1. Selected Bond Lengths (Å) and Angles (deg) for 2a and 2b

	2a	2b
Ru(1)−Ru(2)	2.9492(3)	2.9707(3)
Ru(2)−Ru(3)	2.9616(3)	2.9556(3)
Ru(1)−Ru(4)	2.9785(3)	2.9806(3)
Ru(3)−Ru(4)	2.9671(3)	2.9539(3)
Ru(1)−Ru(3)	2.7875(3)	2.7913(3)
Ru(2)−Ru(4)	2.7775(3)	2.7768(3)
Ru(2)−P(1)	2.3231(7)	
Ru(4)−P(2)	2.3184(7)	
Ru(1)−P(1)		2.3154(7)
Ru(2)−P(2)		2.3168(7)
P(1)−Ru(2)−Ru(4)	171.677(19)	
P(2)−Ru(4)−Ru(2)	168.668(19)	
P(1)−Ru(1)−Ru(2)		115.113(19)
P(2)−Ru(2)−Ru(1)		109.470(19)

to the unbridged Ru−Ru bonds. The two phosphine ligands are coordinated to the two Ru atoms with the normal Ru−P distances [av 2.3184(7) Å]. The two phosphine ligands are found in positions transoid to the short (nonbridged) Ru−Ru bond in **2a** and transoid to the long hydride-bridged Ru−Ru bond in **2b**.

Spectroscopic and Structural Characterization of 3. The spectroscopic data for **3** are fully consistent with the solid-state structure (vide infra). Its FAB mass spectrum displays a parent ion envelope centered at *m*/*z* 1326, and an absorption band at 1722 cm^{-1} in the IR spectrum of **3** confirms the presence of bridging carbonyl ligand. The $^{31}P\{^1H\}$ NMR spectrum consists of three resonances in which the two signals at δ −5.10 and −19.98 ppm correspond to the two σ-bonded phosphines in different environments. A more downfield resonance is also observed at δ 145.52 ppm due to the μ-phosphido ligand. The presence of two metal hydrides can be established using ^1H NMR spectroscopy, and two upfield virtual triplets resonate at δ −14.17 and −18.23 ppm. In the low-field region, all the signals stand for the protons on the furyl groups, which incorporate a manifold series of multiplets in close proximity integrating for 27 protons.

The molecular structure of **3** portrayed in Figure 3 shows that the tetrahedral geometry of the metal framework is retained, one edge of which is bridged by the μ-furylphosphide ligand. The Ru(1)−Ru(4) edge is also spanned by the dissociated furyl ring bonded in a μ-η^1,η^2 fashion. Although there have been several precedents of furyl group coordination through a μ-η^2-vinyl type bridge in dinuclear and multimetallic systems,[10,12] this type of bonding mode is unknown in tetraruthenium clusters. The coordination around the Ru_4 core is completed by two hydride ligands, one bridging and seven terminal CO groups, and two σ-bound phosphine groups to give an outer valence electron count of 60. Two of the Ru−Ru vectors are separately bridged by the

(11) (a) Homanen, P.; Persson, R.; Haukka, M.; Pakkanen, T. A.; Nordlander, E. *Organometallics* **2000**, *19*, 5568. (b) Churchill, M. R.; Lashewycz, R. A.; Shapley, J. R.; Richter, S. I. *Inorg. Chem.* **1980**, *19*, 1277. (c) Wilson, R. D.; Wu, S. M.; Love, R. A.; Bau, R. *Inorg. Chem.* **1978**, *17*, 1271. (d) Sasvari, K.; Main, P.; Frediani, P. *Acta Crystallogr.* **1979**, *B35*, 87. (e) Bianchi, M.; Frediani, P.; Salvini, A.; Rosi, L.; Pistolesi, L.; Piacenti, F.; Ianelli, S.; Nardelli, M. *Organometallics* **1997**, *16*, 482.

(12) (a) Seyferth, D.; Anderson, L. L.; Villafañe, F.; Cowie, M.; Hilts, R. W. *Organometallics* **1992**, *11*, 3262. (b) Dettlaf, G.; Behrens, U.; Eicher, T.; Weiss, E. *J. Organomet. Chem.* **1978**, *152*, 203. (c) Himmelreich, D.; Müller, G. *J. Organomet. Chem.* **1985**, *297*, 341.

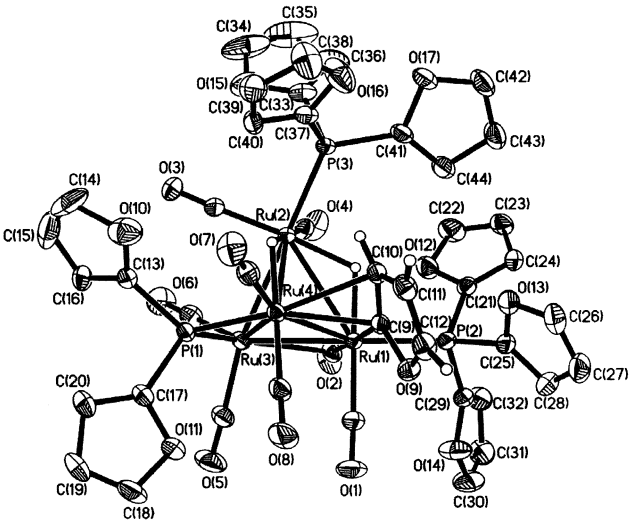

Figure 3. Molecular structure of **3** with 25% probability ellipsoids. For clarity, all H atoms on the furyl rings are omitted and the labels on the carbonyl C atoms have the same labels as the O atoms.

Table 2. Selected Bond Lengths (Å) and Angles (deg) for 3

Ru(1)−Ru(2)	2.9698(3)	Ru(1)−Ru(4)	2.8685(3)
Ru(2)−Ru(4)	3.0112(3)	Ru(3)−Ru(4)	2.9378(3)
Ru(1)−Ru(3)	2.7261(3)	Ru(2)−Ru(3)	2.7611(3)
Ru(1)−P(2)	2.3322(8)	Ru(2)−P(3)	2.3418(7)
Ru(3)−P(1)	2.2030(8)	Ru(4)−P(1)	2.2925(7)
Ru(1)−C(9)	2.057(3)	Ru(4)−C(9)	2.338(3)
Ru(4)−C(10)	2.448(3)	Ru(1)−C(2)	1.964(3)
Ru(3)−C(2)	2.565(3)	C(2)−O(2)	1.126(4)
C(9)−C(10)	1.401(4)		
P(2)−Ru(1)−Ru(2)	118.90(2)	P(3)−Ru(2)−Ru(1)	121.18(2)
Ru(3)−P(1)−Ru(4)	81.59(2)	Ru(1)−C(9)−Ru(4)	81.20(9)
C(9)−Ru(4)−C(10)	33.9(1)	C(9)−Ru(1)−Ru(4)	53.67(8)

phosphido ligand (Ru(3)−Ru(4)) and the furyl group (Ru(1)−Ru(4)), while the Ru(1)−Ru(3) vector in the "basal" plane, which is the shortest Ru−Ru bond, is bridged unsymmetrically by a CO group [Ru(1)−C(2) 1.964(3), Ru(3)−C(2) 2.565(3) Å] (Table 2). The fourth ruthenium atom, Ru(2), caps this plane. The location of the two metal hydrides can be located by X-ray analysis in which they bridge the Ru(1)−Ru(2) (2.9698(3) Å) and Ru(2)−Ru(4) (3.0112(3) Å) edges. These two hydride-bridged metal−metal bonds are somewhat elongated in comparison to the four remaining Ru−Ru distances [2.7261(3)−2.9378(3) Å]. The two substituted phosphines are coordinated to Ru(1) and Ru(2) by the strong Ru−P σ bonds, where the Ru−P distances (2.3322(8) and 2.3418(7) Å, respectively) are notably longer than those in **2a** and **2b**. The phosphide unit is asymmetrically bonded to Ru(3) (2.2030(8) Å) and Ru(4) (2.2925(7) Å). The furyl moiety is σ-attached to Ru(1) [Ru(1)−C(9) 2.057(3) Å] and π-attached to Ru(4) [Ru(4)−C(9) 2.338(3), Ru(4)−C(10) 2.448(3) Å]. The plane consisting of Ru(1), Ru(3), and Ru(4) makes a dihedral angle of 10.8° with the triangular Ru(3)−Ru(4)−P(1) plane. To the best of our knowledge, only five structurally characterized examples are known in the literature for a tetrahedral Ru_4 core bearing μ-phosphido bridges, including $[Ru_4(\mu\text{-}H)_2(CO)_{10}(\mu\text{-}PPh_2)_2]$,[13] $[Ru_4(\mu\text{-}H)(CO)_8(\mu_3\text{-}PPhCH_2PPh_2)(\mu\text{-}\eta^1,\eta^5\text{-}CH_2C_5Me_4)]$,[14] $[Ru_4(\mu\text{-}H)(CO)_9(\mu\text{-}CO)(\mu\text{-}PPh_2)\{\mu_3\text{-}HC_2PPh_2\{(\mu\text{-}H)_4Ru_4(CO)_{11}\}\}]$,[15] $[Ru_4(\mu\text{-}H)_3(CO)_{12}(\mu_3\text{-}PPhCH_2PPh_2)]$,[16] and $[Ru_4(\mu_3\text{-}H)(CO)_{10}\{\mu\text{-}P(NPr^i_2)_2\}(\mu_3\text{-}PNPr^i_2)]$.[17]

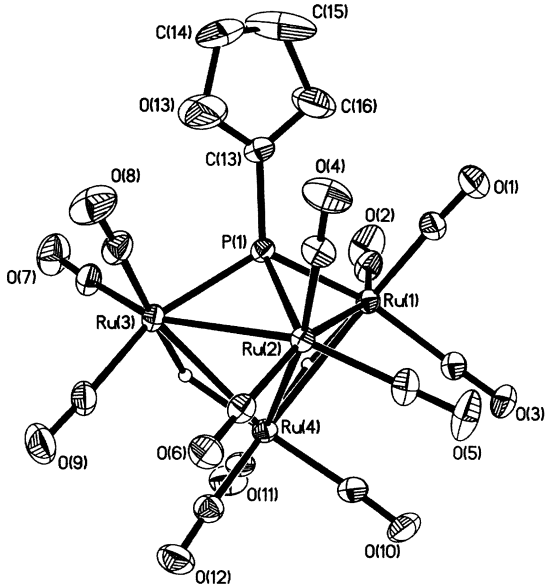

Figure 4. Molecular structure of **4** with 25% probability ellipsoids. For clarity, all H atoms on the furyl rings are omitted and the labels on the carbonyl C atoms have the same labels as the O atoms.

Spectroscopic and Structural Characterization of 4−6. The title reaction has been shown to provide a convenient route to a series of new phosphinidene-stabilized butterfly clusters $[Ru_4(\mu\text{-}H)_2(CO)_{12-x}(PFu_3)_x(\mu_3\text{-}PFu)]$ ($x = 0$ (**4**), 2 (**5**), 3 (**6**)) via cleavage of the Ru−Ru bond and activation of the P−C bond. Each of the FAB mass spectra exhibits the respective parent ion peak as well as signals corresponding to the sequential loss of carbonyl ligands. Their IR spectra suggest the absence of μ-CO ligands, and they exhibit different ν(CO) spectral patterns from each other. The $^{31}P\{^1H\}$ NMR spectra of **4**−**6** display highly deshielded resonances at δ 352.69 (**4**), 338.19 (**5**), and 322.13 ppm (**6**), which are within the normal range for μ_3-phosphinidene ligands in electron-precise Ru_4 clusters.[2f,h,18] For **5** and **6**, another two unresolved high-field resonances located at δ −6.45 and −17.99 ppm for **5** (δ −10.05 and −22.40 ppm for **6**) arise from the two substituted phosphines. The presence of metal hydrides in **4**−**6** can be shown by the high-field signals in their ^1H NMR spectra, which integrate as two protons in each case.

The molecular structures of **4**−**6** are depicted in Figures 4−6, respectively. The structures of **5** and **6** are essentially identical to that of **4**, with the replacement of carbonyls in **4** by two or three PFu_3 groups. Due to their similar structural features, complexes **4**−**6** will not be discussed separately. Their pertinent structural parameters are tabulated in Table 3. These structures show that the original tetrahedral structure of **1** was

(13) Hogarth, G.; Hadj-Bagheri, N.; Taylor, N. J.; Carty, A. J. *Chem. Commun.* **1990**, 1352.

(14) Bruce, M. I.; Humphrey, P. A.; Skelton, B. W.; White, A. H. *J. Organomet. Chem.* **1996**, *522*, 259.

(15) Adams, C. J.; Bruce, M. I.; Skelton, B. W.; White, A. H. *J. Organomet. Chem.* **1992**, *423*, 83.

(16) Bruce, M. I.; Horn, E.; Shawkataly, O. B.; Snow, M. R.; Tiekink, E. R. T.; Williams, M. L. *J. Organomet. Chem.* **1986**, *316*, 187.

(17) Corrigan, J. F.; Doherty, S.; Taylor, N. J.; Carty, A. J. *Organometallics* **1993**, *12*, 993.

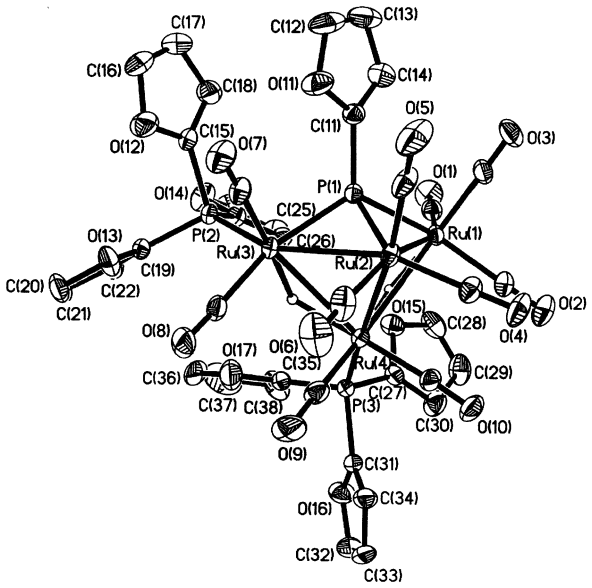

Figure 5. Molecular structure of **5** with 25% probability ellipsoids. For clarity, all H atoms on the furyl rings are omitted and the labels on the carbonyl C atoms have the same labels as the O atoms.

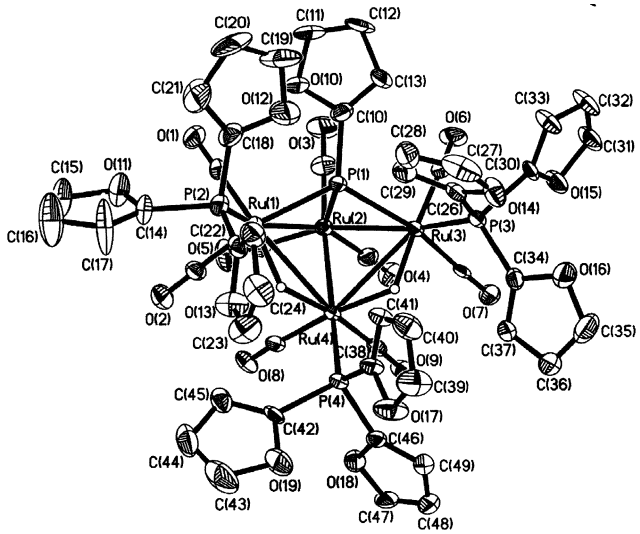

Figure 6. Molecular structure of **6** with 25% probability ellipsoids. For clarity, all H atoms on the furyl rings are omitted and the labels on the carbonyl C atoms have the same labels as the O atoms.

destroyed and the four ruthenium atoms now adopt a 62-electron butterfly skeletal arrangement with the μ_3-phosphinidene ligand capping the open Ru_3 triangle composed of the two wingtip atoms Ru(1) and Ru(3) and the hinge atom Ru(2), which afford a five-vertex polyhedron containing a furylphosphinidene fragment occupying a basal vertex. All carbonyl ligands are in terminal positions. For **5**, two PFu_3 ligands are coordinated to the Ru(3) and Ru(4) atoms by strong Ru−P σ bonds, whereas one additional PFu_3 group is σ-bonded to Ru(1) in **6** to give a trisubstituted product. Although examples of non-hydrido clusters exhibiting a similar μ_3-PR-supported Ru_4 butterfly structure are common,[2c,d,f,4a,18] ruthenium hydrido clusters having this kind of geometry are rare and have been observed only in $[Ru_4(\mu\text{-}H)_2(CO)_{12}(\mu_3\text{-}PPh)]$.[18a] In these three structures, the hydride ligands were located as bridging the two hinge

Table 3. Selected Bond Lengths (Å) and Angles (deg) for 4−6

	4	5	6
Ru(1)−Ru(2)	2.8626(4)	2.8581(3)	2.8675(9)
Ru(1)−Ru(4)	3.0110(4)	3.0132(3)	3.0099(8)
Ru(2)−Ru(3)	2.8534(4)	2.8901(3)	2.8581(9)
Ru(3)−Ru(4)	2.9946(4)	3.0036(3)	3.0207(9)
Ru(2)−Ru(4)	2.8225(4)	2.8171(3)	2.8159(8)
Ru(1)−P(1)	2.2908(8)	2.3027(7)	2.315(2)
Ru(2)−P(1)	2.3607(9)	2.3649(7)	2.379(2)
Ru(3)−P(1)	2.2944(9)	2.3020(7)	2.3177(18)
Ru(X)−P(2)		2.2865(7) (X = 3)	2.292(2) (X = 1)
Ru(Y)−P(3)		2.3074(7) (Y = 4)	2.295(2) (Y = 3)
Ru(Z)−P(4)			2.3195(19) (Z = 4)
Ru(1)−P(1)−Ru(2)	75.95(3)	75.50(2)	75.29(6)
Ru(2)−P(1)−Ru(3)	75.59(3)	76.51(2)	74.95(5)
Ru(1)−P(1)−Ru(3)	123.97(4)	122.86(3)	123.52(8)
P(2)−Ru(A)−Ru(B)		118.897(19) (A = 3, B = 4)	122.30(5) (A = 1, B = 4)
P(3)−Ru(C)−Ru(D)		120.962(18) (C = 4, D = 3)	118.84(5) (C = 3, D = 4)
P(4)−Ru(E)−Ru(F)			172.01(5) (E = 4, F = 2)

to wingtip Ru(1)−Ru(4) and Ru(3)−Ru(4) edges, which are the longest metal−metal bonds in these molecules, while the hinge Ru(2)−Ru(4) bond has the shortest length. The phosphinidene-capped hinge−wingtip edges Ru(1)−Ru(2) and Ru(2)−Ru(3) are typical at 2.8581(3)−2.8675(9) and 2.8534(4)−2.8901(3) Å, respectively. These Ru−Ru distances compare favorably with those in $[Ru_4(\mu\text{-}H)_2(CO)_{12}(\mu_3\text{-}PPh)]$.[18a] The Ru−P(1) distances in **4**−**6** are consistent with a formal assignment of the triply bridged phosphinidene moiety.[18,19] The hinge Ru−P bond lengths (2.3607(9)−2.379(2) Å) are longer than the wingtip Ru−P distances (2.2926(9)−2.316(2) Å), in line with the values found in ruthenium clusters where a phosphinidene ligand caps an open Ru_3 triangular face [2.302−2.395 Å].[18a,19] The dihedral angles between the two wings of the butterfly are very close to each other (75.8°, 76.7°, and 75.2° for **4**, **5**, and **6**, respectively).

Spectroscopic and Structural Characterization of 7. The spectroscopic properties of **7** are consistent with its formulation. Complex **7** displays a FAB mass spectrum exhibiting a molecular ion peak at *m*/*z* 1287. The proton NMR signals arising from the furyl groups are all apparent and integrate to a total of 23 protons against the hydridic protons. The $^{31}P\{^1H\}$ NMR spectrum shows a poorly resolved downfield resonance at δ 228.18 ppm due to the μ_4-phosphinidene P atom and two sets of doublets at δ −15.02 ($^2J_{P-P}$ = 116 Hz) and −20.13 ppm ($^2J_{P-P}$ = 138 Hz) corresponding to the two substituted PFu_3 ligands.

In Figure 7, the structure of **7** consists of a distorted square of Ru atoms that is capped on one side by a μ_4-phosphinidene ligand. On the other side, an unfamiliar furyne ligand formally functions as a four-electron donor bridging three Ru atoms in a μ_3-η^1,η^1,η^2 manner to afford a *nido*-Ru_3C_2 square pyramidal polyhedron such that complex **7** has 64 valence electron counts, as expected for a square metal core. There is no interaction

(18) (a) Van Gastel, F.; Corrigan, J. F.; Doherty, S.; Taylor, N. J.; Carty, A. J. *Inorg. Chem.* **1992**, *31*, 4492. (b) Wang, W.; Enright, G. D.; Driediger, J.; Carty, A. J. *J. Organomet. Chem.* **1997**, *541*, 461. (c) Wang, W.; Corrigan, J. F.; Doherty, S.; Enright, G. D.; Taylor, N. J.; Carty, A. J. *Organometallics* **1996**, *15*, 2770. (d) Corrigan, J. F.; Doherty, S.; Taylor, N. J.; Carty, A. J. *Organometallics* **1992**, *11*, 3160.
(19) (a) Maclaughlin, S. A.; Taylor, N. J.; Carty, A. J. *Can. J. Chem.* **1982**, *60*, 87. (b) Field, J. S.; Haines, R. J.; Smit, D. N. *J. Organomet. Chem.* **1982**, *240*, C23.

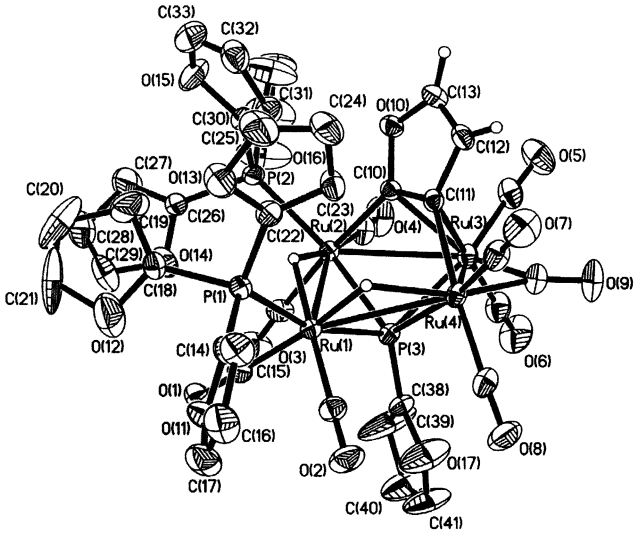

Figure 7. Molecular structure of **7** with 25% probability ellipsoids. For clarity, all H atoms on the furyl rings are omitted and the labels on the carbonyl C atoms have the same labels as the O atoms.

between the furyne oxygen and any part of the metal skeleton. Previously, the cyclic furyne ligand has been isolated in only one instance by Barnes and co-workers in some cyclopentadienyl cobalt clusters where the ring is bound to the cobalt centers through the C_3-C_4 edge,[20] but it has never been observed in clusters of group 8 metal atoms. Indeed, compound **7** is the first example of stable furyne-containing clusters of ruthenium to be structurally characterized and, in this case, coordination of the furyne ligand occurs via a C_2-C_3 bond instead. The coordination mode of the furyne ring here appears different from that observed in the two structurally related non-hydrido clusters $[Ru_4(CO)_{11}(\mu_4\text{-PPh})(\mu_4\text{-}C_4H_2S)]$, where the thiophyne moiety is bonded to the Ru_4 base in a $\mu_4\text{-}\eta^1,\eta^1,\eta^2,\eta^2$ fashion,[6a] and $[Ru_4(CO)_{11}\text{-}(\mu_4\text{-PPh})(\mu_4\text{-}C_4H_3N)]$, where an analogous C,C-bonded pyrrolyne ligand is present.[6c] The four metal atoms in **7** are distorted from a planar arrangement by the presence of bridging ligands. The planar furyne ring makes a dihedral angle of 60.9° with the Ru_4 mean plane, and the coordinated C−C bond is diagonally disposed across the Ru_4 square. Complexation of the five-membered furyne ring causes appreciable elongation of the unsaturated C−C separation to 1.385(5) Å, which is attributed to back π-bonding into the π^* orbitals of the alkyne unit, and this distance is close to the value of 1.374(9) Å found in $[Cp_3Co_3(CO)(\mu_3\text{-}\eta^2\text{-}C_4H_4O)]$.[20] The length of the C(12)−C(13) bond corresponds to a normal double bond. Cluster **7** has one symmetric μ-CO ligand along the edge Ru(3)−Ru(4) (Ru(3)−C(9) 2.039(4), Ru(4)−C(9) 2.070(4) Å). The Ru−Ru distances span the range 2.7399(5)−3.0734(4) Å, and the Ru(2) and Ru(4) centers in the basal positions of the *nido*-M_3C_2 system each form a σ bond with C(10) (Ru(2)−C(10) 2.097(4) Å) and C(11) (Ru(4)−C(11) 2.142(4) Å) atoms of the five-membered ring, respectively. The C(10)−C(11) edge also participates in a π-interaction to the Ru(3) vertex in the apical position.

Table 4. Selected Bond Lengths (Å) and Angles (deg) for 7

Ru(1)−Ru(2)	3.0734(4)	Ru(2)−Ru(3)	2.9985(5)
Ru(3)−Ru(4)	2.7399(5)	Ru(1)−Ru(4)	3.0444(4)
Ru(1)−P(1)	2.3462(10)	Ru(2)−P(2)	2.3460(11)
Ru(1)−P(3)	2.3230(10)	Ru(2)−P(3)	2.3969(10)
Ru(3)−P(3)	2.4856(11)	Ru(4)−P(3)	2.4296(10)
Ru(2)−C(10)	2.097(4)	Ru(3)−C(10)	2.323(4)
Ru(3)−C(11)	2.312(3)	Ru(4)−C(11)	2.142(4)
C(10)−C(11)	1.385(5)	C(12)−C(13)	1.319(6)
Ru(1)−P(3)−Ru(2)	81.24(3)	Ru(1)−P(3)−Ru(3)	130.09(4)
Ru(1)−P(3)−Ru(4)	79.64(3)	Ru(2)−P(3)−Ru(3)	75.75(3)
Ru(2)−P(3)−Ru(4)	109.52(4)	Ru(3)−P(3)−Ru(4)	67.75(3)
P(1)−Ru(1)−Ru(2)	119.44(3)	P(2)−Ru(2)−Ru(1)	109.60(3)
Ru(2)−C(10)−C(11)	129.4(3)	C(10)−Ru(3)−C(11)	34.78(12)
Ru(4)−Ru(3)−C(10)	76.21(9)	Ru(4)−Ru(3)−C(11)	49.29(9)

Table 5. Electrochemical Data of 2a and 3−7

	oxidation[a]			reduction[a]	
cluster	E_{pa1}/V	E_{pa2}/V	E_{pa3}/V	E_{pc1}/V	E_{pc2}/V
2a	+0.46 (1)	+0.70 (1)	+0.87 (1)		
3	+0.27 (1)	+0.53 (1)	+0.83 (1)	−1.56 (2)	
4	+1.01 (2)			−1.44 (1)	−1.63 (1)
5	+0.67 (2)				
6	+0.42 (2)				
7	+0.59 (1)				

[a] E_{pa} and E_{pc} are the anodic and cathodic potentials, respectively (vs $Ag/AgNO_3$). Values in parentheses are faraday/mol of the cluster.

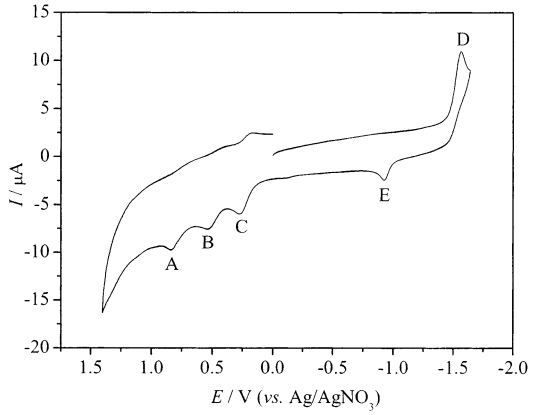

Figure 8. Cyclic voltammogram of **3** measured in CH_2Cl_2 solution (scan rate 100 mV s^{-1}).

Electrochemistry. The electrochemical properties of our new organotetraruthenium clusters were investigated in CH_2Cl_2 by cyclic voltammetry (CV), and the data are summarized in Table 5. Cluster **3** has a rich redox chemistry, and the cyclic voltammogram of **3** contains three consecutive irreversible anodic waves at +0.27 (A), +0.53 (B), and +0.83 V (C) (vs $Ag/AgNO_3$) with approximately equal peak currents (Figure 8). An increased scan rate did not lead to any noticeable reversibility of the redox couple. The irreversible nature of oxidation is presumably derived from an irreversible chemical reaction that follows the redox reaction; that is, it conforms to an ECECEC process.[21] Controlled-potential coulometry (CPC) was performed at the working potential (E_w) of +0.98 V for **3**, showing that three electrons are removed for each molecule. On the basis of the relative peak heights, each anodic wave is

(20) (a) Barnes, C. E.; King, W. D.; Orvis, J. A. *J. Am. Chem. Soc.* **1995**, *117*, 1855. (b) King, W. D.; Barnes, C. E.; Orvis, J. A. *Organometallics* **1997**, *16*, 2152.

(21) (a) Drake, S. R. *Polyhedron* **1990**, *9*, 455. (b) Cyr, J. E.; Rieger, P. H. *Organometallics* **1991**, *10*, 2153. (c) Osella, D.; Ravera, M.; Nervi, C.; Housecroft, C. E.; Raithby, P. R.; Zanello, P.; Laschi, F. *Organometallics* **1991**, *10*, 3253.

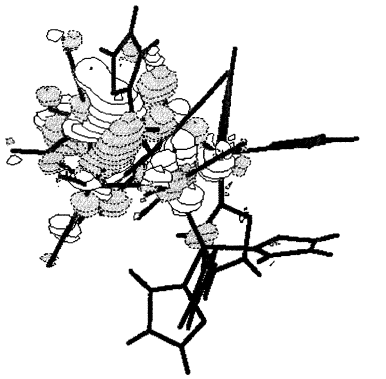

LUMO

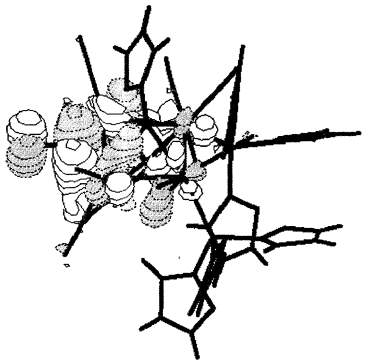

HOMO

Figure 9. Spatial plots of the highest occupied (HOMO) and lowest unoccupied (LUMO) molecular orbitals for **7**.

tentatively assigned to have consumed one electron. It also shows an irreversible two-electron reduction wave at −1.56 V (D), and associated with this wave is the reoxidation peak at −0.93 V (E), i.e., the oxidation wave of the reduced product. The region where the weak return oxidation peak appears was initially empty, with the wave appearing after the cathodic wave traversed. The electrochemical behavior of **3** is different from those of **5** and **7** on the CV time scale. Cluster **5** exhibits an irreversible two-electron oxidation step at +0.67 V, whereas **7** an irreversible single-electron oxidation event at +0.59 V. No cathodic wave was located within the solvent limit for both **5** and **7**. It was observed that the potential of the first oxidation peak for **3** is much lower than those found in **5** and **7**, and the results are in line with theoretical calculations obtained by the method of density functional theory (DFT). DFT calculations at the B3LYP level show that the unbridged Ru−Ru σ-bonding molecular orbitals, slightly mixed with π* orbitals of the carbonyl ligands, are lying in the HOMO region, while the corresponding σ* and metal−ligand σ*(d) orbitals dominate the LUMO region (Figure 9). Mulliken population analysis[22] shows that the metal contributions to the HOMO and LUMO are large in all cases (e.g., HOMO 60.9, 54.4, 52.2%; LUMO 48.7, 45.6, 45.8% for **3**, **5**, and **7**, respectively). The fact that both the HOMO and LUMO levels in each case are predominantly metal in character suggests that smaller HOMO−LUMO gaps (E_{gap}) are indicative of weaker metal−metal interactions.[21a] The theoretical results are thus consistent with redox processes leading to a perturbation of the Ru_4 core rather than of any other part of the molecule. The calculated E_{gap} values are 2.68, 3.34, and 3.60 eV for **3**, **5**, and **7**, respectively. The larger E_{gap} values for **5** and **7** are a manifestation of the fact that both μ_3-PR and μ_4-PR groups tend to stabilize the respective HOMO level, leading to a lower ease of oxidation. The lower LUMO level due to the smaller E_{gap} for **3** also accounts for the observation of a reduction peak in **3**, which is, however, absent in **5** and **7**. The strongly Ru−Ru σ*-antibonding character for the LUMO in **3** is in line with metal−metal bond cleavage concerted with or following reduction. For **4**, **5**, and **6**, which differ by the extent of phosphine coordination in the metal framework, each of them undergoes a single irreversible oxidation event and bulk electrolyses indicate that exactly 2 faradays/mol of each molecule is involved in each electron transfer step according to a four-component ECEC mechanism to yield the corresponding dication. Again, the order of the first oxidation potential **4** (+1.01) > **5** (+0.67) > **6** (+0.42 V) is consistent with the replacement of carbonyl groups by successive PFu_3 ligands (having a higher σ donor/π acceptor ratio), which results in a sufficient increase in electron density on the Ru atoms to raise the energy of the HOMO level from **4** to **5** to **6**. With regard to reduction, as the number of phosphine ligands increases, the reduction potentials are expected to shift cathodically, and so only the cathodic peaks of **4** are located within the solvent limits at −1.44 and −1.63 V. This could be taken to be indicative of an increase in energy of the LUMO caused by inductive effects due to the P donor ligands. The fact that the redox potentials are sensitive to the electronic effects of the ligands on the Ru_4 frame suggests that the oxidation and reduction events concern mainly the metallic core. While cluster **2a** displays three one-electron-transfer steps as confirmed by CPC, the less positive oxidation potentials of **3** as compared to **2a** are in accord with the presence of strong Ru−C(furyl) σ-bonding, which may weaken the Ru−Ru bonding interactions and push up the HOMO level in **3**. The observation of a reduction wave for **3** suggests that the bridging units significantly lower the LUMO of the cluster and make the reduction easier. These results also agree with the DFT-estimated E_{gap} values for **2a** (3.51 eV) and **3** (2.68 eV).

Concluding Remarks

This report shows that the functionalized tri(2-furyl)-phosphine is a versatile synthon in tetraruthenium carbonyl clusters affording a range of new tetraruthenium dihydrido carbonyl clusters containing μ-phosphide and μ_3- and μ_4-phosphinidene ligands. In this one-pot reaction, the usefulness of such furyl-substituted phosphines to open up a novel synthetic strategy to furnish new metallophosphorus clusters has been demonstrated, and remarkably for this type of reaction there is apparently little or no cluster fragmentation. Similar to the thiophene counterpart,[23] even though furan (C_4H_4O) is relatively weakly coordinated to metals, its derivatives, furyl (C_4H_3O) and furyne (C_4H_2O) ligands,

(22) *MullPop*, a program written by Reinaldo Pis Diez at the National University of La Plata, Argentina.

(23) Arce, A. J.; Deeming, A. J.; Sanctis, Y. D.; Speel, D. M.; Trapani, A. D. *J. Organomet. Chem.* **1999**, *580*, 370.

are shown to be capable of binding strongly to metal atoms in carbonyl clusters. Structural characterization of complexes **3** and **7** constitutes the first examples of compounds of the iron triad that are coordinated by the μ-η^1,η^2-furyl and μ_3-η^1,η^1,η^2-furyne fragments, respectively. The work presented here also provides another interesting example of the ability of an assembly of transition metal atoms to stabilize metastable furyne ligands. The correlation between the redox behavior and the molecular orbital calculations of these complexes was established in the present study. The observation that μ_3- and μ_4-PFu ligands stabilize the HOMO toward oxidation seems in keeping with the general use of these groups as cluster-stabilizing fragments.

Experimental Section

General Comments. All reactions were conducted under an atmosphere of dry nitrogen with the use of standard Schlenk techniques. Solvents for preparative work were dried and distilled before use. $[Ru_4(\mu\text{-}H)_4(CO)_{12}]$ was prepared according to the reported procedures.[24] IR spectra were obtained using a Nicolet FTIR-550 spectrometer. NMR spectra were recorded in $CDCl_3$ on a JEOL JNM-EX 270 or a Varian Inova 400 MHz FT-NMR spectrometer. Fast atom bombardment (FAB) mass spectra were recorded on a Finnigan-SSQ 710 spectrometer. Electrochemical measurements were performed with an EG&G Princeton Applied Research (PAR) model 273A potentiostat. Cyclic voltammograms were obtained using an argon gas sealed two-compartment cell equipped with a glassy carbon working electrode, a platinum wire auxiliary electrode, and an $Ag/AgNO_3$ reference electrode at room temperature at a scan rate of 100 mV s^{-1}. The solvent in all measurements was deoxygenated CH_2Cl_2, and the supporting electrolyte was 0.1 M $[Bu_4N]PF_6$. Ferrocene was added as an internal standard at the end of each experiment. Bulk electrolyses were carried out at room temperature in a gastight cell consisting of three chambers separated at the bottom by fine frits, with a carbon cloth (80 mm^2) working electrode in the middle and $Ag/AgNO_3$ reference and Pt gauze auxiliary electrodes in the lateral chambers. The working potential (E_w) for the redox processes was ca. 0.15 V more positive/negative than the corresponding electrode potential (E_p). All coulometric experiments were performed in duplicate. Density functional calculations at the B3LYP level[25] were performed on the new clusters on the basis of their experimentally determined geometries obtained from crystallographic data. The basis set used for C, O, and H atoms was 6-31G,[26] while effective core potentials with a LanL2DZ basis set[27] were employed for Ru and P atoms. A polarization function was added for P atoms ($\zeta_d = 0.34$). The Gaussian 98 program was used for the calculations.

Thermal Reaction of $[Ru_4(\mu\text{-}H)_4(CO)_{12}]$ with Tri(2-furyl)phosphine. Tri(2-furyl)phosphine (31.4 mg, 0.135 mmol) was added to a solution of $[Ru_4(\mu\text{-}H)_4(CO)_{12}]$ (100 mg, 0.134 mmol) in THF (30 mL), and reflux of the solution for 3 h resulted in a marked color change from yellow to reddish-brown. Upon removal of solvent, the residue was first subjected to preparative TLC on silica gel using hexane−CH_2Cl_2 (9:1, v/v) as eluent to give two yellow-orange bands, which were identified as the clusters $[Ru_4(\mu\text{-}H)_2(CO)_{12}(\mu_3\text{-}PFu)]$ (**4**, R_f = 0.60) and $[Ru_4(\mu\text{-}H)_4(CO)_{10}(PFu_3)_2]$ (**2b**, $R_f = 0.38$). A group of closely spaced bands with R_f values in the range 0.05−0.14 was chromatographed again on silica plates eluting with hexane−CH_2Cl_2 (1:1, v/v) to afford five more bands. In order of elution, these compounds were $[Ru_4(\mu\text{-}H)_4(CO)_{10}(PFu_3)_2]$ (**2a**, R_f = 0.66), $[Ru_4(\mu\text{-}H)_2(CO)_{10}(PFu_3)_2(\mu_3\text{-}PFu)]$ (**5**, R_f = 0.49), $[Ru_4(\mu\text{-}H)_2(CO)_8(PFu_3)_2(\mu\text{-}PFu_2)(\mu\text{-}\eta^1,\eta^2\text{-}C_4H_3O)]$ (**3**, $R_f = 0.31$), $[Ru_4(\mu\text{-}H)_2(CO)_9(PFu_3)_2(\mu_4\text{-}PFu)(\mu_3\text{-}\eta^1,\eta^1,\eta^2\text{-}C_4H_2O)]$ (**7**, R_f = 0.29), and $[Ru_4(\mu\text{-}H)_2(CO)_9(PFu_3)_3(\mu_3\text{-}PFu)]$ (**6**, $R_f = 0.23$).

2a: red solid. Yield: 41.7 mg (27%). IR (CH_2Cl_2): ν(CO) 2078(s), 2058(vs), 2038(s), 2022(vs), 1998(s), 1964(w) cm^{-1}. ^1H NMR ($CDCl_3$): δ −17.16, −16.45 (br, 4H, Ru-H), 6.44 (m, 6H, Fu), 6.66 (m, 6H, Fu), 7.64 (s, 6H, Fu). $^{31}P\{^1H\}$ NMR ($CDCl_3$): δ −16.16. FAB-MS (*m*/*z*): 1152 [M^+]. Anal. Calcd for $C_{34}H_{22}O_{16}P_2Ru_4$: C, 35.43; H, 1.92. Found: C, 35.20; H, 2.01.

2b: orange-red solid. Yield: 7.8 mg (5%). IR (CH_2Cl_2): ν(CO) 2078(s), 2058(vs), 2038(s), 2022(vs), 1998(s), and 1962(w) cm^{-1}. ^1H NMR ($CDCl_3$): δ −16.96 (t, 4H, Ru-H), 6.51 (m, 6H, Fu), 6.79 (m, 6H, Fu), 7.72 (s, 6H, Fu). $^{31}P\{^1H\}$ NMR ($CDCl_3$): δ −18.59. FAB-MS (*m*/*z*): 1152 [M^+]. Anal. Calcd for $C_{34}H_{22}O_{16}P_2Ru_4$: C, 35.43; H, 1.92. Found: C, 35.11; H, 2.04.

3: deep red solid. Yield: 26.7 mg (15%). IR (CH_2Cl_2): ν(CO) 2063(vw), 2044(m), 2016(vs), 1972(m), 1963(m), 1917(w), 1722(br) cm^{-1}. ^1H NMR ($CDCl_3$): δ −18.23 (t, 1H, Ru-H), −14.17 (t, 1H, Ru-H), 3.42 (d, 1H, Fu), 5.43 (m, 1H, Fu), 6.03 (m, 1H, Fu), 6.18 (m, 1H, Fu), 6.28 (m, 6H, Fu), 6.36 (m, 1H, Fu), 6.43 (m, 3H, Fu), 6.61 (m, 3H, Fu), 6.76 (m, 2H, Fu), 7.43 (s, 3H, Fu), 7.47 (s, 3H, Fu), 7.53 (s, 1H, Fu), 7.57 (s, 1H, Fu). $^{31}P\{^1H\}$ NMR ($CDCl_3$): δ −19.98, −5.10 (PFu_3), 145.52 (μ-PFu_2). FAB-MS (*m*/*z*): 1326 [M^+]. Anal. Calcd for $C_{44}H_{29}O_{17}P_3Ru_4$: C, 39.83; H, 2.20. Found: C, 39.68; H, 2.14.

4: orange solid. Yield: 13.7 mg (12%). IR (CH_2Cl_2): ν(CO) 2104(w), 2079(vs), 2066(vs), 2032(vs), 1973(w) cm^{-1}. ^1H NMR ($CDCl_3$): δ −19.24 (d, 1H, Ru-H), −17.79 (s, 1H, Ru-H), 6.51 (m, 1H, Fu), 6.98 (t, 1H, Fu), 7.70 (s, 1H, Fu). $^{31}P\{^1H\}$ NMR ($CDCl_3$): δ 352.69 (μ_3-PFu). FAB-MS (*m*/*z*): 840 [M^+]. Anal. Calcd for $C_{16}H_5O_{13}PRu_4$: C, 22.87; H, 0.60. Found: C, 22.62; H, 0.55.

5: red solid. Yield: 16.7 mg (10%). IR (CH_2Cl_2): ν(CO) 2075(m), 2043(vs), 2025(s), 2006(m), 1986(sh), 1970(sh) cm^{-1}. ^1H NMR ($CDCl_3$): δ −18.45 (t, 1H, Ru-H), −17.55 (m, 1H, Ru-H), 6.26 (m, 6H, Fu), 6.44 (m, 1H, Fu), 6.53 (m, 6H, Fu), 6.66 (m, 1H, Fu), 7.48 (m, 6H, Fu), 7.60 (s, 1H, Fu). $^{31}P\{^1H\}$ NMR ($CDCl_3$): δ −17.99, −6.45 (PFu_3), 338.19 (μ_3-PFu). FAB-MS (*m*/*z*): 1248 [M^+]. Anal. Calcd for $C_{38}H_{23}O_{17}P_3Ru_4$: C, 36.55; H, 1.86. Found: C, 36.33; H, 1.99.

6: red solid. Yield: 11.68 mg (6%). IR (CH_2Cl_2): ν(CO) 2065(w), 2051(s), 2029(vs), 2016(s), 1987(br), 1976(m) cm^{-1}. ^1H NMR ($CDCl_3$): δ −17.27 (m, 2H, Ru-H), 6.05 (m, 3H, Fu), 6.14 (m, 6H, Fu), 6.46 (m, 3H, Fu), 6.53 (s, 1H, Fu), 6.57 (m, 6H, Fu), 7.23 (m, 3H, Fu), 7.31−7.48 (m, 7H, Fu), 7.61 (s, 1H, Fu). $^{31}P\{^1H\}$ NMR ($CDCl_3$): δ −22.40, −10.05 (PFu_3), 322.13 (μ_3-PFu). FAB-MS (*m*/*z*): 1453 [M^+]. Anal. Calcd for $C_{49}H_{32}O_{19}P_4Ru_4$: C, 40.51; H, 2.22. Found: C, 40.32; H, 2.40.

7: red-orange solid. Yield: 13.80 mg (8%). IR (CH_2Cl_2): ν(CO) 2063(m), 2042(s), 2028(vs), 2008(vs), 1969(m), 1794(w) cm^{-1}. ^1H NMR ($CDCl_3$): δ −16.34 (m, 1H, Ru-H), −14.79 (m, 1H, Ru−H), 6.19−6.30 (m, 9H, Fu), 6.55 (m, 5H, Fu), 6.64 (s, 1H, Fu), 7.04 (m, 1H, Fu), 7.21 (s, 1H, Fu), 7.47 (m, 5H, Fu), 7.69 (s, 1H, Fu). $^{31}P\{^1H\}$ NMR ($CDCl_3$): δ −20.13 (d, $^2J_{P-P}$ = 138 Hz, PFu_3), −15.02 (d, $^2J_{P-P}$ = 116 Hz, PFu_3), 228.18 (m, μ_4-PFu). FAB-MS (*m*/*z*): 1287 [M^+]. Anal. Calcd for $C_{41}H_{25}O_{17}P_3Ru_4$: C, 38.27; H, 1.96. Found: C, 38.06; H, 1.88.

Crystallography. Suitable crystals of **2a**, **2b**, **3**, **4**, **5**, **6**, and **7** suitable for X-ray diffraction analyses were grown by slow evaporation of their respective solutions in a hexane−CH_2Cl_2 mixture. Geometric and intensity data were collected using graphite-monochromated Mo Kα radiation (λ = 0.71073 Å) on a Bruker AXS SMART CCD area-detector diffractometer. The collected frames were processed with the software SAINT,[28] and an absorption correction based on the SADABS program

(24) Knox, S. A. R.; Koepke, J. W.; Andrews, M. A.; Kaesz, H. D. *J. Am. Chem. Soc.* **1975**, *97*, 3942.
(25) (a) Decke, A. D. *J. Chem. Phys.* **1993**, *98*, 5648. (b) Miehlich, B.; Savin, A.; Stoll, H.; Preuss, H. *Chem. Phys. Lett.* **1989**, *157*, 200. (c) Lee, C.; Yang, W.; Parr, G. *Phys. Rev. B* **1988**, *37*, 785.
(26) Hariharan, P. C.; Pople, J. A. *Theor. Chim. Acta* **1973**, *28*, 213.
(27) Hay, P. J.; Wadt, W. R. *J. Chem. Phys.* **1985**, *82*, 299.
(28) *SAINT Reference Manual*; Siemens Energy and Automation: Madison, WI, 1994−1996.

Table 6. Crystal Data for Complexes 2a, 2b, and 3−7

	2a	2b	3	4	5	6·C_5H_{12}·H_2O	7
empirical formula	$C_{34}H_{22}O_{16}P_2Ru_4$	$C_{34}H_{22}O_{16}P_2Ru_4$	$C_{44}H_{29}O_{17}P_3Ru_4$	$C_{16}H_5O_{13}PRu_4$	$C_{38}H_{23}O_{17}P_3Ru_4$	$C_{49}H_{32}O_{19}P_4Ru_4$·$C_5H_{12}$·$H_2O$	$C_{41}H_{25}O_{17}P_3Ru_4$
fw	1152.74	1152.74	1326.86	840.45	1248.75	1543.07	1286.80
cryst size, mm	0.32 × 0.18 × 0.15	0.28 × 0.16 × 0.12	0.30 × 0.10 × 0.08	0.30 × 0.21 × 0.18	0.29 × 0.24 × 0.09	0.28 × 0.18 × 0.12	0.34 × 0.19 × 0.17
cryst syst	triclinic	monoclinic	monoclinic	monoclinic	triclinic	triclinic	monoclinic
space group	$P\bar{1}$	$P2_1/c$	$P2_1/n$	$P2_1/c$	$P\bar{1}$	$P\bar{1}$	$C2/c$
a, Å	9.3836(6)	13.2376(8)	18.8059(10)	17.2846(11)	10.7244(7)	11.392(2)	37.575(3)
b, Å	14.6876(10)	18.2880(11)	12.6525(7)	8.6028(6)	11.6046(7)	11.981(2)	12.6602(9)
c, Å	15.6481(10)	17.5132(11)	20.7120(11)	16.7755(11)	18.3353(11)	22.082(4)	19.4740(13)
α, deg	94.9460(10)				84.9080(10)	92.445(4)	
β, deg	97.2530(10)	109.4390(10)	108.4100(10)	104.9940(10)	88.2640(10)	101.154(4)	98.8300(10)
γ, deg	107.2810(10)				74.2740(10)	90.597(4)	
V, Å^3	2025.3(2)	3998.1(4)	4676.0(4)	2409.5(3)	2187.7(2)	2953.9(9)	9154.1(11)
Z	2	4	4	4	2	2	8
D_{calcd}, g cm^{-3}	1.890	1.915	1.885	2.317	1.896	1.735	1.867
μ, mm^{-1}	1.610	1.631	1.443	2.586	1.535	1.185	1.471
F(000)	1120	2240	2600	1584	1216	1532	5024
θ range, deg	1.32−27.53	1.63−27.52	1.77−27.52	2.44−27.53	1.83−27.50	1.82−25.00	1.96−27.51
no. of reflns collected	11 764	23 170	26 769	13 661	12 833	14 965	26 566
no. of unique reflns	8545	8966	10 461	5433	9333	10 252	10 303
R(int)	0.0108	0.0259	0.0200	0.0250	0.0135	0.0624	0.0304
no. of reflns with $I > 2.0\sigma(I)$	7813	7032	8658	4797	8146	4891	7383
no. of params	522	522	622	320	568	726	595
R1, wR2 [$I > 2.0\sigma(I)$][a]	0.0220, 0.0587	0.0242, 0.0493	0.0250, 0.0666	0.0269, 0.0725	0.0247, 0.0679	0.0611, 0.1299	0.0343, 0.0854
R1, wR2 (all data)	0.0251, 0.0648	0.0371, 0.0536	0.0340, 0.0736	0.0313, 0.0755	0.0294, 0.0717	0.1349, 0.1520	0.0539, 0.0930
goodness of fit	1.098	0.958	0.859	1.031	0.889	0.841	0.880
largest diff peak and hole, e Å^{-3}	0.478 and −0.577	0.484 and −0.368	0.595 and −0.418	1.135 and −0.883	0.600 and −0.458	0.859 and −1.573	1.021 and −0.711

[a] $R1 = \sum||F_o| - |F_c||/\sum|F_o|$. $wR2 = \{\sum[w(F_o^2 - F_c^2)^2]/\sum[w(F_o^2)^2]\}^{1/2}$.

was applied.[29] The structure was solved by the direct methods (SHELXTL)[30] in conjunction with standard difference Fourier techniques and subsequently refined by full-matrix least-squares analyses. All non-hydrogen atoms were assigned with anisotropic displacement parameters. The hydride atom positions were located from Fourier maps, and those hydrogen atoms on the furyl rings were generated in their idealized positions and allowed to ride on the respective carbon atoms. Crystallographic and other experimental details are collected in Table 6.

(29) Sheldrick, G. M. *SADABS*, Empirical Absorption Correction Program; University of Göttingen: Germany, 1997.

(30) Sheldrick, G. M. *SHELXTL Reference Manual*, version 5.1; Siemens Energy and Automation: Madison, WI, 1997.

Acknowledgment. We thank the Hong Kong Baptist University (Grant No. FRG/01-02/I-31) for financial support, and F.-L.T. acknowledges the receipt of a studentship administered by the Hong Kong Baptist University.

Supporting Information Available: Details of data collection parameters, bond lengths, bond angles, fractional atomic coordinates, and anisotropic thermal parameters for all new complexes are available free of charge via the Internet at http://pubs.acs.org.

OM0341193